

Homoleptic Diphosphacyclobutadiene Complexes $[M(\eta^4\text{-P}_2\text{C}_2\text{R}_2)_2]^x-$ ($M = \text{Fe, Co}$; $x = 0, 1$)

Robert Wolf,^{*,[a, b]} Andreas W. Ehlers,^[b] Marat M. Khusniyarov,^[c] František Hartl,^[d, e]
Bas de Bruin,^[d] Gary J. Long,^[f] Fernande Grandjean,^[g] Falko M. Schappacher,^[a]
Rainer Pöttgen,^[a] J. Chris Slootweg,^[b] Martin Lutz,^[h] Anthony L. Spek,^[h] and
Koop Lammertsma^{*,[b]}

Abstract: The preparation and comprehensive characterization of a series of homoleptic sandwich complexes containing diphosphacyclobutadiene ligands are reported. Compounds $[\text{K}([\text{18}]\text{crown-6})(\text{thf})_2][\text{Fe}(\eta^4\text{-P}_2\text{C}_2\text{tBu}_2)_2]$ (**K1**), $[\text{K}([\text{18}]\text{crown-6})(\text{thf})_2][\text{Co}(\eta^4\text{-P}_2\text{C}_2\text{tBu}_2)_2]$ (**K2**), and $[\text{K}([\text{18}]\text{crown-6})(\text{thf})_2][\text{Co}(\eta^4\text{-P}_2\text{C}_2\text{Ad}_2)_2]$ (**K3**, Ad = adamantyl) were obtained from reactions of $[\text{K}([\text{18}]\text{crown-6})(\text{thf})_2][\text{M}(\eta^4\text{-C}_{14}\text{H}_{10})_2]$ ($M = \text{Fe, Co}$) with $t\text{BuC}\equiv\text{P}$ (**1**, **2**), or with $\text{AdC}\equiv\text{P}$ (**3**). Neutral sandwiches

$[\text{M}(\eta^4\text{-P}_2\text{C}_2\text{tBu}_2)_2]$ (**4**: $M = \text{Fe}$ **5**: $M = \text{Co}$) were obtained by oxidizing **1** and **2** with $[\text{Cp}_2\text{Fe}]\text{PF}_6$. Cyclic voltammetry and spectro-electrochemistry indicate that the two $[\text{M}(\eta^4\text{-P}_2\text{C}_2\text{tBu}_2)_2]^-/[\text{M}(\eta^4\text{-P}_2\text{C}_2\text{tBu}_2)_2]$ moieties can be reversibly interconverted by one electron oxidation and reduction, respectively. Complexes **1–5** were characterized by multi-nuclear NMR, EPR (**1** and **5**), UV/Vis,

and Mössbauer spectroscopies (**1** and **4**), mass spectrometry (**4** and **5**), and microanalysis (**1–3**). The molecular structures of **1–5** were determined by using X-ray crystallography. Essentially D_{2d} -symmetric structures were found for all five complexes, which show the two 1,3-diphosphacyclobutadiene rings in a staggered orientation. Density functional theory calculations revealed the importance of covalent metal–ligand π bonding in **1–5**. Possible oxidation state assignments for the metal ions are discussed.

Keywords: cobalt • iron • metalates • phosphorus • sandwich complexes

[a] Dr. R. Wolf, Dr. F. M. Schappacher, Prof. Dr. R. Pöttgen
Institute of Inorganic and Analytical Chemistry
University of Münster
Corrensstrasse 30, 48149 Münster (Germany)
Fax: (+49) 251-833-6610
E-mail: r.wolf@uni-muenster.de

[b] Dr. R. Wolf, Dr. A. W. Ehlers, Dr. J. C. Slootweg,
Prof. Dr. K. Lammertsma
Department of Organic and Inorganic Chemistry
Faculty of Sciences, VU University Amsterdam
De Boelelaan 1083, 1081 HV, Amsterdam (The Netherlands)
Fax: (+31) 20-5987488
E-mail: K.Lammertsma@few.vu.nl

[c] Dr. M. M. Khusniyarov
Department of Chemistry and Pharmacy
Friedrich-Alexander-Universität Erlangen-Nürnberg
Egerlandstrasse 1, 91058 Erlangen (Germany)


[d] Prof. Dr. F. Hartl, Dr. B. de Bruin
Homogeneous and Supramolecular Catalysis
Van't Hoff Institute for Molecular Sciences
University of Amsterdam
Science Park 904, 1098 XH Amsterdam (The Netherlands)

[e] Prof. Dr. F. Hartl
Department of Chemistry, University of Reading
Whiteknights, Reading, RG6 6AD (UK)

[f] Prof. Dr. G. J. Long
Department of Chemistry
Missouri University of Science and Technology
University of Missouri, Rolla, MO 65409-0010 (USA)

[g] Prof. Dr. F. Grandjean
Department of Physics, B5, University of Liège
4000 Sart-Tilman (Belgium)

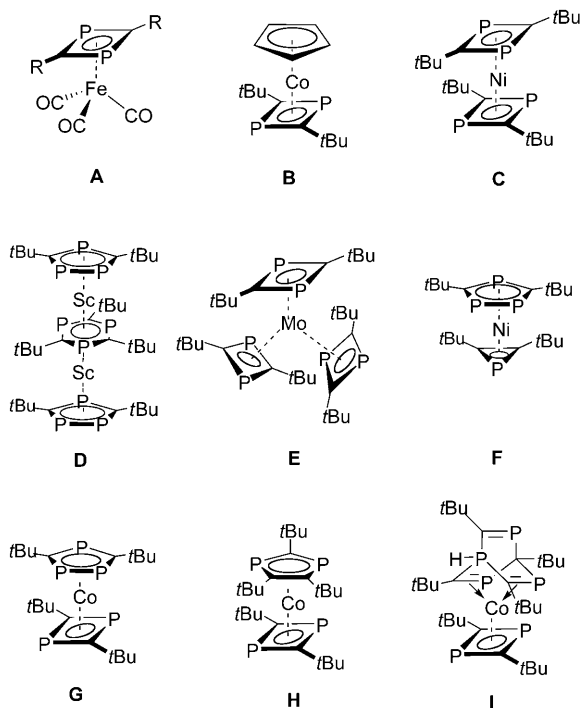
[h] Dr. M. Lutz, Prof. Dr. A. L. Spek
Bijvoet Center for Biomolecular Research
Crystal and Structural Chemistry, Utrecht University
Padualaan 8, 3584 CH, Utrecht (The Netherlands)

 Supporting information for this article is available on the WWW under <http://dx.doi.org/10.1002/chem.201001913>.

Introduction

Since the discovery of ferrocene, $[\text{Cp}_2\text{Fe}]$, sandwich complexes have fascinated the chemical community. Sandwiches containing cyclopentadienyl and arene ligands are most common. In particular, ferrocene derivatives have found numerous applications.^[1,2] The chemistry of complexes containing four-membered cyclobutadiene rings is comparatively less developed.^[3,4] In particular, the paucity of homoleptic cyclobutadiene complexes is striking.^[5]

Phosphaalkynes, such as *tert*-butylphosphaalkyne ($t\text{Bu}-\text{C}\equiv\text{P}$), can undergo transition-metal-mediated cyclooligomerization, which is a versatile method that can generate complexes with phosphaorganic ligands.^[6,7] Cyclodimerization to heteroleptic 1,3-diphosphacyclobutadiene complexes is frequently encountered. For example, the reaction of $[\text{Fe}(\text{CO})_5]$ with $t\text{Bu}-\text{C}\equiv\text{P}$ results in the formation of complex **A**, a phosphorus analogue of Petit's complex $[\text{Fe}(\eta^4-\text{C}_4\text{H}_4)(\text{CO})_3]$.^[8] By using cyclopentadienyl half-sandwich complexes, for example, $[\text{CpCo}(\eta^2-\text{C}_2\text{H}_2)_2]$, heteroleptic complexes, such as **B**, are formed.^[9] Complex **C**, which has been prepared from $[\text{Ni}(\eta^4-\text{cod})_2]$ and $t\text{Bu}-\text{C}\equiv\text{P}$, represents the only homoleptic diphosphacyclobutadiene complex reported prior to our work.^[10]



Unique and structurally diverse products, for example, complexes **D–F**, can be obtained by using “gaseous” metal atoms that are accessible by means of metal vapor (MV) synthesis.^[11] Unfortunately, the applicability of metal vapor synthesis is limited by the poor selectivity, low yields, and the special experimental apparatus required. Product mix-

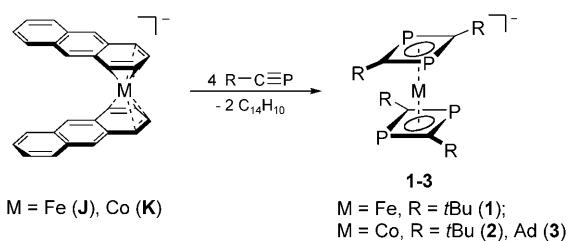
tures are often formed. For example, the reaction of “gaseous” cobalt atoms with $t\text{Bu}-\text{C}\equiv\text{P}$ yielded three complexes **G–I**, which contain diphosphacyclobutadiene, phosphacyclopentadienyl ligands, and a protonated tetraphosphabarrelene.^[12]

Considering the fascinating products that are obtained from reactions of “gaseous” metal atoms with phosphaalkynes we reasoned that unprecedented anionic sandwich complexes could be synthesized by using “naked” transition-metal anions. Ellis and co-workers have recently shown that reactive arene metalates may serve as efficient synthetic equivalents for M^{n-} synthons.^[13] The preparation of the decaphosphatitanocene dianion $[\text{Ti}(\eta^5-\text{P}_5)_2]^{2-}$ by means of the reaction of an anionic titanium naphthalene complex with P_4 is a striking illustration of the potential of such compounds.^[14] Apart from this landmark example, arene metalates have not been utilized for the preparation of organometallic sandwich compounds. Therefore, we endeavored to study reactions of homoleptic metalates with phosphaalkynes. Here we report a full account of our preliminary studies.^[15] First, we describe the synthesis of the anionic diphosphacyclobutadiene sandwich complexes $[\text{K}([\text{18}]\text{crown-6})(\text{thf})_2][\text{Fe}(\eta^4-\text{P}_2\text{C}_2t\text{Bu}_2)_2]$ (**K1**), $[\text{K}([\text{18}]\text{crown-6})(\text{thf})_2][\text{Co}(\eta^4-\text{P}_2\text{C}_2t\text{Bu}_2)_2]$ (**K2**), and $[\text{K}([\text{18}]\text{crown-6})(\text{thf})_2][\text{Co}(\eta^4-\text{P}_2\text{C}_2\text{Ad}_2)_2]$ (**K3**, Ad = adamantyl) the structures and spectroscopic properties of which are discussed. Second, we present an analysis of the redox properties of anions **1** and **2**. We describe the synthesis of the neutral oxidation products $[\text{Fe}(\eta^4-\text{P}_2\text{C}_2t\text{Bu}_2)_2]$ (**4**) and $[\text{Co}(\eta^4-\text{P}_2\text{C}_2t\text{Bu}_2)_2]$ (**5**), which may be considered as rare phosphorus analogues of elusive bis(cyclobutadiene) complexes $[\text{Fe}(\eta^4-\text{C}_4\text{R}_4)_2]$ and $[\text{Co}(\eta^4-\text{C}_4\text{R}_4)_2]$. Third, we report the Mössbauer spectra of **1** and **4** and analyze DFT calculations for model compounds, which provide, for the first time, detailed insight into the electronic structures of homoleptic diphosphacyclobutadiene complexes.

Results and Discussion

Syntheses, structures and spectroscopic properties of the anionic sandwich complexes K1–K3: Orange potassium salts $[\text{K}([\text{18}]\text{crown-6})(\text{thf})_2][\text{Fe}(\eta^4-\text{P}_2\text{C}_2t\text{Bu}_2)_2]$ (**K1**), $[\text{K}([\text{18}]\text{crown-6})(\text{thf})_2][\text{Co}(\eta^4-\text{P}_2\text{C}_2t\text{Bu}_2)_2]$ (**K2**), and $[\text{K}([\text{18}]\text{crown-6})(\text{thf})_2][\text{Co}(\eta^4-\text{P}_2\text{C}_2\text{Ad}_2)_2]$ (**K3**) were obtained in moderate to good yields by reacting four equivalents of phosphaalkyne ($t\text{Bu}-\text{C}\equiv\text{P}$ or $\text{Ad}-\text{C}\equiv\text{P}$)^[16,17] with the metalates $[\text{Fe}(\eta^4-\text{C}_{14}\text{H}_{10})_2]^-$ (**J**) and $[\text{Co}(\eta^4-\text{C}_{14}\text{H}_{10})_2]^-$ (**K**, Scheme 1).^[18,19] Although highly sensitive to moisture and oxygen, all three compounds are thermally very robust and decompose at temperatures above 230 °C.

The identity of **K1–K3** was established by X-ray crystallography, microanalyses, EPR (**1**), NMR, and UV/Vis spectroscopies. In the solid state, all three compounds show similar ion-separated structures that comprise homoleptic anions $[\text{Fe}(\eta^4-\text{P}_2\text{C}_2t\text{Bu}_2)_2]^-$ (**1**), $[\text{Co}(\eta^4-\text{P}_2\text{C}_2t\text{Bu}_2)_2]^-$ (**2**), and $[\text{Co}(\eta^4-\text{P}_2\text{C}_2\text{Ad}_2)_2]^-$ (**3**), as well as a $[\text{K}([\text{18}]\text{crown-6})(\text{thf})_2]^+$



Scheme 1.

counteraction.^[18,19] The molecular structure of adamantyl-substituted **K3** is shown as an example in Figure 1. The anions feature two η^4 -coordinated diphosphacyclobutadiene rings in a staggered orientation, owing to the steric repulsion of the *t*Bu (**1**, **2**) or Ad (**3**) substituents. The P_2C_2 rings of

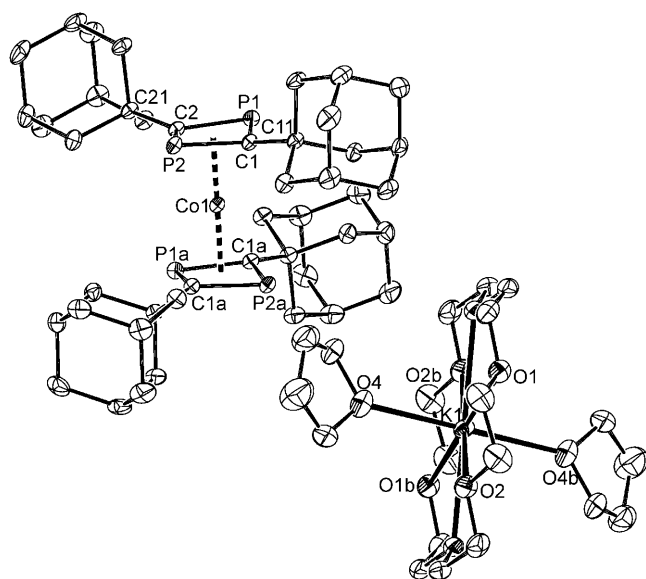


Figure 1. Solid-state structure of $[K([18]\text{crown-6})(\text{thf})_2][\text{Co}(\eta^4\text{-P}_2\text{C}_2\text{Ad}_2)_2]$ (**K3**), displacement ellipsoids at 50% probability level, H atoms and disordered solvent molecules are omitted for clarity. Symmetry equivalents used to generate equivalent atoms: a) $1-x, 0.5-z$; b) $1.5-x, 0.5-y, -z$.

the ligands display equal P–C bond lengths (Table 1). The P–C bond lengths (1.7999(18)–1.8028(18) Å) are typical for 1,3-diphosphacyclobutadienes coordinated to first row transition metals.^[6] Metal–phosphorus and metal–carbon bond lengths are in the range reported for related, neutral complexes, for example, **A–C**.^[8–10,20] The Fe–P and Fe–C bond lengths in the iron complex **1** are slightly larger than the

Co–P and Co–C bond lengths in the cobalt species **2** and **3**, due to the larger radius of iron.

$[\text{Fe}(\eta^4\text{-P}_2\text{C}_2\text{tBu}_2)_2]^-$ (**1**) is a paramagnetic 17-electron species. The magnetic moment, determined by the Evans method in $[\text{D}_8]\text{THF}$ solution, of $1.77 \mu_B$ indicates the presence of one unpaired electron per iron center. In accordance with the paramagnetism of **1**, only a broad signal in the ^1H NMR spectrum (C_6D_6) was detected for the *t*Bu groups at $\delta \approx -1.9$ ppm. The experimental EPR spectrum of a frozen THF solution ($T = 40$ K, Figure 2) revealed an axial,

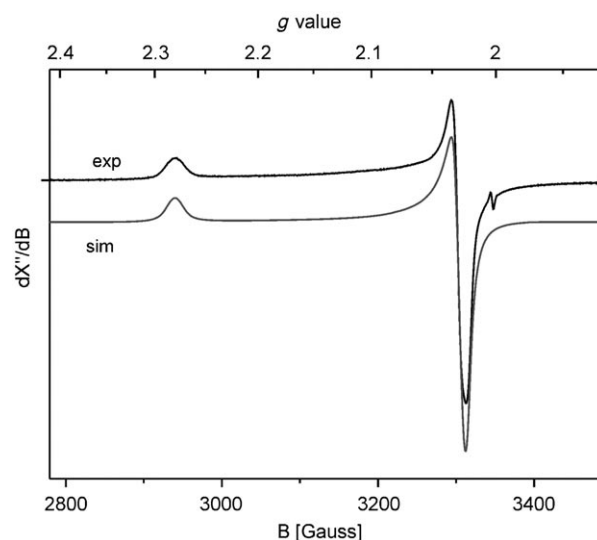


Figure 2. Experimental and simulated X-band EPR spectra of anionic complex **1**. Experimental conditions: $T = 40$ K, attenuation = 30 dB, field modulation amplitude = 4 G, microwave frequency = 9.380276 GHz.

g -tensor, without any resolved hyperfine couplings with the ^{31}P nuclei. A satisfactory spectral simulation was obtained with the g values $g_{11} = 2.279$, $g_{22} = 2.026$, and $g_{33} = 2.026$. The observed pattern is typical for an axially symmetric d^9 species with one unpaired electron and thus further confirms the $S = 1/2$ (doublet) ground state. The EPR properties were also calculated with ADF (OPBE/TZ2P) by using the optimized geometry of $[\text{Fe}(\eta^4\text{-P}_2\text{C}_2\text{Me}_2)_2]^-$ (**1'**) as a smaller computational model of the experimental system. The agreements between the experimental EPR parameters and the DFT-calculated parameters are very reasonable (Table 2).

The related heteroleptic 17-electron complexes $[\text{Fe}(\eta^6\text{-C}_7\text{H}_8)(\eta^4\text{-P}_2\text{C}_2\text{tBu}_2)_2]^+$ ($g_{11} = 2.53$, $g_{22} = g_{33} = 2.01$) and $[\text{Fe}(\eta^5\text{-P}_2\text{C}_3\text{tBu}_3)_2(\eta^4\text{-P}_2\text{C}_2\text{tBu}_2)_2]^-$ ($g_{11} = 2.407$, $g_{22} = g_{33} = 2.026$), described by Zenneck and co-workers,^[21] display similar EPR spectra as **1**, with no observable ^{31}P hyperfine coupling. The

Table 1. Selected bond lengths [Å] and angles [°] of **1–5**.

	K1 ^[15]	K2 ^[15]	K3	4 ^[15]	5
M–P	2.2969(5)–2.3024(5)	2.2537(6)–2.2598(6)	2.2601(5)–2.2620(4)	2.3044(10)–2.3081(9)	2.2811(7)–2.2830(7)
M–C	2.0939(16)–2.1027(16)	2.0649(19)–2.0724(19)	2.0603(17)–2.0671(18)	2.090(3)–2.100(3)	2.086(2)–2.087(2)
P–C	1.8000(17)–1.8048(17)	1.791(2)–1.798(2)	1.7999(18)–1.8028(18)	1.796(3)–1.808(3)	1.801(2)
P–C–P	98.71(8)–99.07(8)	98.66(10)–99.02(10)	99.03(8), 99.03(8)	97.98(15)–98.61(15)	98.66(11)–98.81(11)
C–P–C	80.60(8)–80.94(8)	80.79(9)–81.02(9)	80.61(8), 80.67(8)	80.91(15)–81.41(15)	80.83(11)–80.99(11)

Table 2. Experimental and DFT-calculated EPR parameters of **1** and **5**.

	1		5	
	Exp ^[a]	OPBE/ TZ2P ^[b]	Exp ^[a]	B3LYP/ TZ2P ^[c]
g_{11}	2.279	2.346	2.642	2.317
g_{22}	2.026	2.028	2.038	2.063
g_{33}	2.026	2.024	2.038	2.061
A_{11}^P	NR ^[e]	4×-24	NR ^[e]	4×-31
	< 30			4×-19
A_{22}^P	NR ^[e]	$4 \times +16$	NR ^[e]	$4 \times +12$
	< 20			$4 \times +8$
A_{33}^P	NR ^[e]	$4 \times +24$	NR ^[e]	$4 \times +8$
	< 20			$4 \times +21$
A_{11}^{Co}	–	–	118	+476
A_{22}^{Co}	–	–	NR ^[e]	+468
			< 20	–8
A_{33}^{Co}	–	–	NR ^[e]	–51
			< 20	+48

[a] Parameters from spectral simulations (least squares ‘best fit’). Hyperfine couplings in MHz. [b] DFT-calculated parameters for $[\text{Fe}(\eta^4\text{-P}_2\text{C}_2\text{Me}_2)_2]^-$ (**1**’, ADF, OPBE, TZ2P). [c] DFT-calculated parameters of **5** (optimized with Turbomole, BP86/SV(P), EPR parameters calculated with ADF, OPBE/TZ2P). [d] DFT-calculated parameters of **5** (optimized with Turbomole, B3LYP/TZVP, EPR parameters calculated with ORCA, B3LYP/TZVP). [e] Not resolved (NR) in the experimental X-band spectra.

significant g anisotropies indicate that the unpaired electron is metal-centered in all three cases. This is nicely confirmed for **1** by our DFT calculations (see below). In contrast, the 19-electron anion $[\text{Fe}(\eta^6\text{-C}_7\text{H}_8)(\eta^4\text{-P}_2\text{C}_2\text{tBu}_2)_2]^-$ ($g_{11}=2.032$, $g_{22}=1.992$, and $g_{33}=1.946$) displays a much smaller g anisotropy and thus seems to be a primarily ligand-centered radical.^[21]

The cobaltate anions $[\text{Co}(\eta^4\text{-P}_2\text{C}_2\text{tBu}_2)_2]^-$ (**2**) and $[\text{Co}(\eta^4\text{-P}_2\text{C}_2\text{Ad}_2)_2]^-$ (**3**) are diamagnetic 18-electron complexes. Multinuclear NMR spectroscopy supports the structural formulations obtained from the X-ray crystal structure analysis. Both complexes gave rise to one singlet in the $^{31}\text{P}\{^1\text{H}\}$ NMR spectrum (**K2**: $\delta = +2.4$ ppm, **K3**: $\delta = -2.6$ ppm). ^1H and $^{13}\text{C}\{^1\text{H}\}$ NMR spectra of **K2** showed a single *t*Bu environment. Only one set of adamantyl signals was detected in the

$^{13}\text{C}\{^1\text{H}\}$ NMR spectrum, confirming the highly symmetric nature of **K3**. The UV/Vis spectrum of iron complex **1** in THF showed two intense absorptions in the UV region at $\lambda = 296$ and 383 nm. In addition, a very weak, broad absorption was detected at $\lambda = 699$ nm. The cobaltates **K2** and **K3** displayed very similar UV/Vis spectra in THF with intense absorptions in the UV around $\lambda = 290$ and 330 nm. TD-DFT calculations at the spin-unrestricted B3LYP level of theory indicate that these absorptions mainly arise as a result of charge transfer between occupied metal-centered orbitals and empty ligand orbitals, that is metal-to-ligand charge transfer (MLCT).

Spectro-electrochemistry of complexes 1 and 2: Redox activity is an important facet of organometallic sandwich compounds. Anionic complexes **1** and **2** display identical 1,3-diphospha-2,4-*tert*-butylcyclobutadiene ligands, but differ in the metal center (Fe vs. Co) and electron count (17 e vs. 18 e). Therefore, we decided to perform a comparative study of their redox properties. First, we investigated the redox behavior of **1** and **2** by cyclic voltammetry (CV) in THF. Both complexes are reversibly oxidized at low potentials (**1**: $E_{1/2} = -0.97$ V, **2**: $E_{1/2} = -0.73$ V vs. Fc/Fc^+ , Figure 3, inset). The iron-containing 17-electron anion **1** is oxidized even more easily than the 18-electron cobalt complex **2**.^[22] The electrode potential of the reversible Co redox couple **2/5** (18 $e/17e$) shifts with the solvent polarity, the HOMO of **2** being apparently stabilized in more polar solvents: $E_{1/2}$ (V vs. Fc/Fc^+) = -0.62 in MeCN, -0.68 in CD_2Cl_2 , and -0.73 in THF. Furthermore, the CV spectra of **2**, in CD_2Cl_2 recorded at 213 K, revealed a new, irreversible one-electron wave at $E_{\text{pc}} = -2.70$ V versus Fc/Fc^+ . This cathodic step might indicate the formation of the 19-electron complex $[\text{Co}(\eta^4\text{-P}_2\text{C}_2\text{tBu}_2)_2]^{2-}$ that is highly unstable.

Characterization of oxidized complexes 4 and 5: Subsequent synthetic investigations led to the access of the neutral species **4** and **5** on a preparative scale by oxidizing anions **1** and **2** with $[\text{Cp}_2\text{Fe}]\text{PF}_6$ (Scheme 2). The by-product ferrocene is

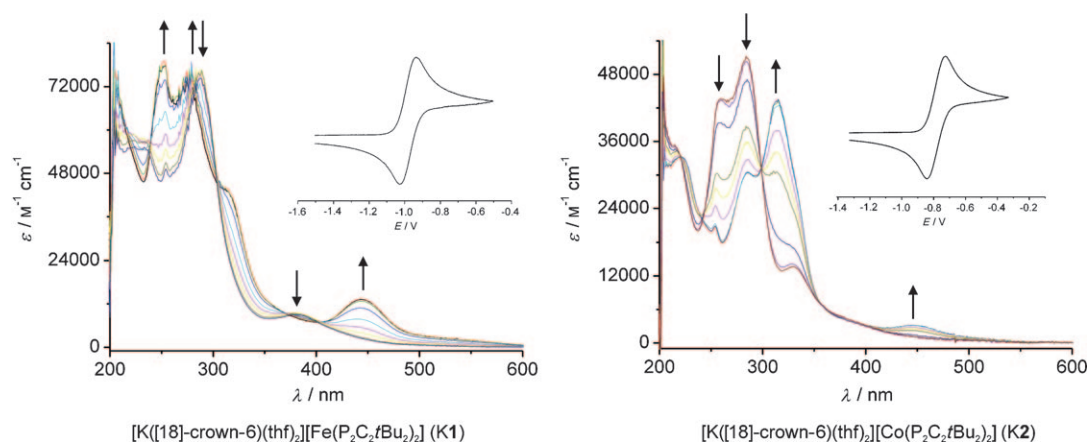
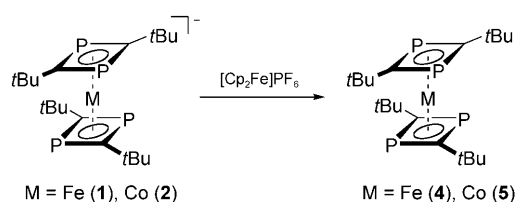


Figure 3. UV/Vis monitoring of the electrochemical oxidation of **1** and **2** in THF/ Bu_4NPF_6 in an OTTLE cell, insets: cyclic voltammograms of **1** and **2** in THF/ Bu_4NPF_6 .



Scheme 2.

easily removed by vacuum sublimation. Complexes **4** and **5** were isolated in moderate yield as orange crystals that are highly soluble in *n*-pentane. Their identity was established by using mass spectrometry, ^1H NMR and EPR spectroscopies, and single-crystal X-ray structure analyses.

Isostructural complexes **4** and **5** crystallize in the monoclinic space group *C2/c* with four molecules in the unit cell.^[15] The structure of **5** is depicted in Figure 4. The mole-

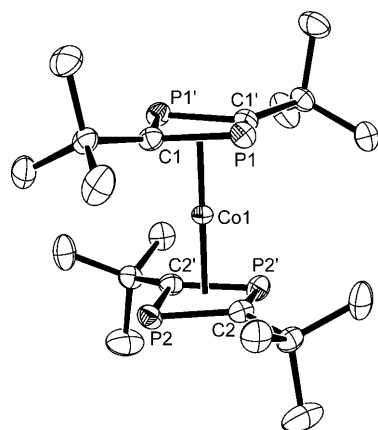


Figure 4. Solid-state structure of $[\text{Co}(\eta^4\text{-P}_2\text{C}_2\text{tBu}_2)_2]$ (**5**). Displacement ellipsoids at 50% probability level, H atoms omitted for clarity.

cules reside on crystallographic C_2 axes, and feature η^4 -coordinated diphosphacyclobutadiene ligands in a staggered orientation. The P–C bond lengths in the rhombic P_2C_2 rings are equal within experimental error (Table 1). The M–P and M–C bond lengths of **4** are marginally longer (0.01–0.02 Å) than in **5**. Comparison of anionic and neutral sandwich structures **1–3** reveals that removing one electron from the anions only has negligible structural effects. In fact, the bond lengths of neutral 16e iron complex **4** are mostly identical to those of the 17-electron anion **1** within experimental error. Co–P and Co–C bond lengths of 17-electron **5** are only slightly longer than those of 18-electron **1** by about 0.02 Å.

Compound **4** is a rare example of a 16-electron iron complex with P-heterocyclic ligands.^[23] The solution magnetic moment of **4** (Evans method, C_6D_6 solution) of $2.74 \mu_{\text{B}}$ is close to the expected spin-only value for two unpaired electrons ($2.82 \mu_{\text{B}}$). This is in accord with our DFT calculations, which predict a triplet ground state (vide infra). Owing to its paramagnetic nature, the ^1H NMR spectrum of **4** in

$[\text{D}_6]\text{benzene}$ featured a broad signal at $\delta = 2.6$ ppm for the *t*Bu groups, whereas the ^1H NMR spectrum of cobalt complex **5** gave rise to a very broad *t*Bu signal at $\delta = -2.6$ ppm in C_6D_6 . Its solution magnetic moment of $1.73 \mu_{\text{B}}$ (determined in the same solvent) perfectly matches the expected spin-only value for one unpaired electron in a low-spin complex.

The UV/Vis spectrum of **4** in THF shows intense absorptions in the UV region with a maximum at $\lambda = 275$ nm and a shoulder at $\lambda = 320$ nm, and a broad medium-intensity absorption band at $\lambda = 443$ nm ($\epsilon_{\text{max}} = 11000 \text{ M}^{-1} \text{ cm}^{-1}$) tailing down to $\lambda = 600$ nm. The electronic absorption spectra of the isoelectronic 17-electron species **1** and **5** feature a remarkably similar pattern. Absorptions of **5** at $\lambda = 313$ and at 440 nm are bathochromically shifted compared to the bands observed for **1** at $\lambda = 296$ and 383 nm (Figure 3).

The EPR spectrum of Co compound **5** revealed an axial *g* tensor, again without any resolved hyperfine couplings with the four ^{31}P nuclei, but with resolved hyperfine coupling with ^{59}Co ($I = 7/2$) along g_{11} (Figure 5). A satisfactory spectral simulation was obtained with the following parameters: $g_{11} = 2.642$, $g_{22} = g_{33} = 2.038$, and $A_{11}^{\text{Co}} = 118 \text{ MHz}$.

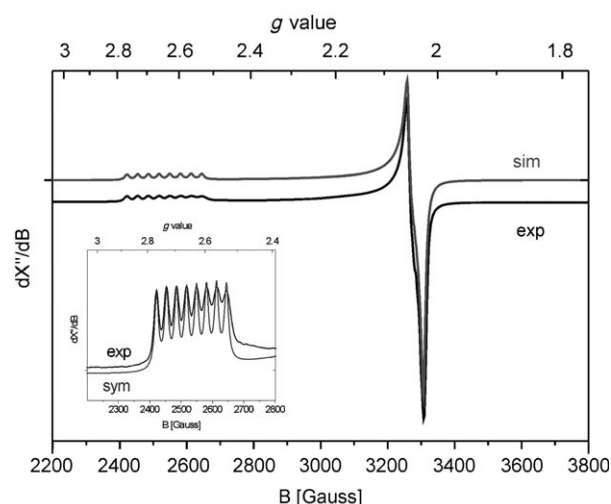


Figure 5. Experimental and simulated X-band EPR spectra of neutral Co complex **5** (inset: expanded area of the spectrum showing the hyperfine coupling to the ^{59}Co nucleus). Experimental conditions: Temperature = 50 K, microwave power 0.2 mW, field modulation amplitude = 2 Gauss, microwave frequency = 9.382254 GHz. The simulated spectrum was obtained with the parameters shown in Table 2.

In an attempt to gain a more detailed understanding of the electronic structure of **5**, we performed DFT EPR property calculations. We used both ADF and ORCA for this purpose. ORCA allowed us to use the hybrid B3LYP functional for these calculations. The EPR parameters of Co complex **5** are not predicted very well (Table 2), neither by ORCA nor by ADF. The DFT calculations in all cases predict much too low g_{11} values and too large A_{11}^{Co} values. It is also clear that slight variations in the structure (Me_4 model versus *t*Bu₄ model) and geometry (optimized at OPBE,

BP86 or B3LYP levels of theory) have a huge influence on the DFT calculated EPR parameters. The poor performance of both ADF and ORCA in predicting the EPR parameters of complex **5** is perhaps not surprising. DFT EPR property predictions are typically poor in cases with nearly degenerate metal centered orbitals, leading to large g_{11} values (as is the case for **5**), for which small geometrical changes have a large influence on the orbital splittings.^[24]

The relatively large g anisotropy and the substantial hyperfine coupling observed for **5** is typical for a metal-centered radical. Related (tetrahedral) d^9 cobalt(0) complexes display smaller g_{11} values, but larger hyperfine couplings.^[25] Smaller g anisotropies than for **5** have been observed for various 19-electron cobalt complexes.^[26] The 19e formally cobalt(0) species $[\text{CpCo}(\text{CO})_2]^-$ displays g values ($g_{11}=2.018$, $g_{22}=1.995$, $g_{33}=2.041$) close to the free electron value g_e and thus seems to be a ligand radical complex.^[27]

Mössbauer spectra of complexes 1 and 4: The ^{57}Fe Mössbauer spectra of **1** have been measured between 4.2 and 265 K and some of the spectra are shown in Figure 6. Two aspects of the spectra are rather unusual. First, the quadrupole doublet has very different component line widths and, second, there is very little change in the absorption profile with temperature. At this point it is important to note that virtually identical spectra have been obtained for three sep-

arate absorbers made from two separate preparations of **1** in two different laboratories; hence, the spectra are reproducible.

Although one might expect more dramatic changes in the line shape with changing temperature, the spectral profiles shown in Figure 6 are indicative of the onset of slow paramagnetic relaxation of the effective hyperfine field associated with the low-spin $S=1/2$ ground state of **1**. As a consequence of the line shape, the spectra have been fit with a relaxation profile based on the formalism developed by Dattagupta and Blume, and an Arrhenius plot of the resulting relaxation rates is shown in Figure S1 of the Supporting Information.^[28,29] The results of these fits are shown as the solid lines in Figure 6. The resulting parameters are given in Table 3, a graphical representation of the temperature de-

Table 3. ^{57}Fe Mössbauer spectroscopic parameters for **1** and **4**.

Complex	T [K]	δ [mm s ⁻¹] ^[a]	$e^2Qq/2$ [mm s ⁻¹]	ν [MHz]	Spectral area [(% ϵ) (mm s ⁻¹)] ^[b]
1	265 ^[c]	0.360	-1.144	245(20)	1.276
	225 ^[c]	0.378	-1.139	220(10)	1.784
	155 ^[c]	0.410	-1.145	205(5)	3.126
	85 ^[c]	0.431	-1.156	168(7)	4.882
	4.2 ^[c]	0.433	-1.163	171(5)	7.550
1 in frozen solution	80 ^[c]	0.63(2)	-0.75(4)	33(1)	–
	80 ^[d]	0.61(2)	-0.80(4)	36(1)	–
4	77 ^[c]	0.309	1.30	–	1.689

[a] The isomer shifts are given relative to 295 K α -iron powder. [b] % ϵ indicates % effect. [c] Line width fixed at 0.30 mm s⁻¹. [d] Line width fixed at 0.385 mm s⁻¹.

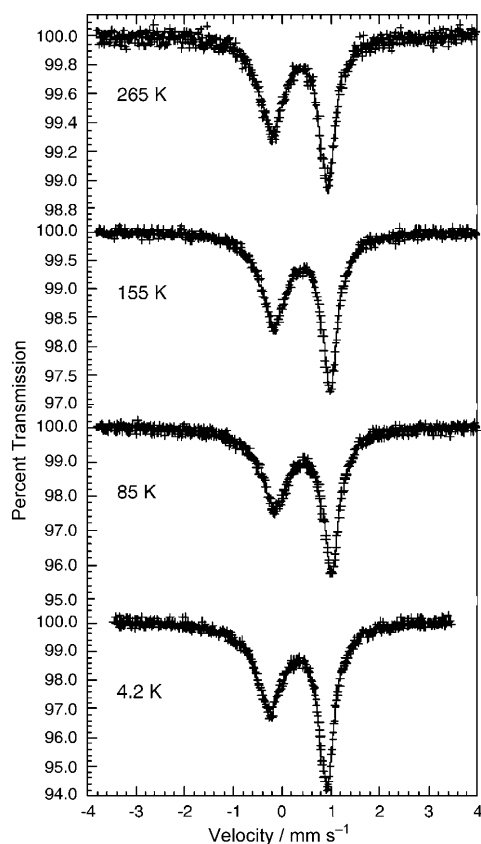


Figure 6. The ^{57}Fe Mössbauer spectra of **1** obtained at the indicated temperatures and fit with a relaxation profile.

pendencies is given in Figure S2. The relaxation frequency is essentially the same upon warming from 4.2 to 85 K and increases slightly between 85 and 265 K; the observed temperature dependence is consistent with the presence of spin-spin mediated relaxation in **1** as a result of intermolecular iron-iron magnetic exchange interactions. The temperature dependence of the isomer shift of **1** is well fit with the Debye model^[30] for the second-order Doppler shift with a characteristic Mössbauer temperature, Θ_M , of 604(17) K, a value that is reasonable for the environment of the low-spin iron(III) ion, and the temperature dependence of the spectral area yields a Debye temperature, Θ_D , of 134(3) K (for a graphical representation see Figure S2 in the Supporting Information).^[31]

To confirm that the relaxation observed in the Mössbauer spectra of **1** is mediated by spin-spin interactions, the spectrum of **1** has also been measured at 80 K in a frozen THF solution. The resulting spectrum (see Figure S3 in the Supporting Information) has been fit with the same relaxation model as used above with a fixed line width of 0.30 mm s⁻¹ and a fixed hyperfine field of 11 T; a slightly better fit may be obtained if the line width is increased to 0.385 mm s⁻¹. The parameters derived from these fits are given in Table 3. It is clear from these results that the relaxation rate is sub-

stantially reduced in the frozen solution, as compared with the bulk sample, as a result of the dramatically increased iron–iron distance. This results in a reduction in the spin–spin interactions and thus the spin–spin mediation of the relaxation. It is also apparent that in the frozen solution the magnitude of the quadrupole interaction is somewhat reduced and, more surprisingly, the isomer shift is increased more than might be expected.

In contrast to **1**, the Mössbauer spectrum of **4** obtained at 77 K is a simple symmetric quadrupole doublet (see Figure S4 in the Supporting Information) with a line width of 0.30 mm s^{−1}; the spectral hyperfine parameters are given in Table 3. The isomer shifts of **1** are similar to those observed for ferrocenium-like low-spin iron(III) complexes.^[33,34] It is noteworthy that the observed isomer shift for **4** is somewhat smaller than that of **1**, a decrease that agrees with and supports the calculated values (see Table 4). It is immediately

Table 4. Calculated Mössbauer spectral parameters.^[a]

Complex	$\rho(0)$ [a.u. ^{−3}]	$\rho(0)$ [Å ^{−3}]	$\delta_{\text{Fe}}^{[b]}$ [mm s ^{−1}]	$V_{zz}^{[c]}$ [V m ^{−2}]	$eQV_{zz}/2^{[c]}$ [mm s ^{−1}]	η
[Fe(P ₂ C ₂ Me ₂) ₂] ^{2−}	11816.43(2)	79730.9(1)	0.520(5)	$-15.92(3) \times 10^{21}$	+2.65(1)	0
[Fe(P ₂ C ₂ Me ₂) ₂] [−] , 1'	11816.83(2)	79733.5(1)	0.375(5)	$+4.15(3) \times 10^{21}$	−0.69(1)	0
[Fe(P ₂ C ₂ Me ₂) ₂], 4'	11816.87(2)	79733.9(1)	0.360(5)	$-7.81(3) \times 10^{21}$	+1.81(1)	0

[a] The parameters have been obtained from spin-unrestricted B3LYP-DFT calculations. [b] The isomer shifts are given relative to α -iron, and calculated^[53] from $\delta_{\text{Fe}} = -0.367(\rho(0) - 11800) + 6.55$. [c] 1×10^{21} V m^{−2} corresponds to a $(eQV_{zz})/2$ of 0.166 mm s^{−1} for a nuclear quadrupole moment of $0.16(1) \times 10^{-28}$ m².

apparent from this table that there is good qualitative agreement with the observed results given in Table 3. Furthermore, it is not surprising that the asymmetry parameter η is zero for both complexes, owing to D_{2d} symmetry. In contrast, it is rather unexpected that a one-electron d_{z^2} -centered oxidation results only in a minor increase of the isomer shift. This can be nicely explained by our theoretical calculations, which show that the electron populations of the d_{xz} and d_{yz} orbitals increase significantly after the loss of one electron from the d_{z^2} orbital on oxidation (vide infra), a loss that decreases their s-electron shielding, increases the s-electron density at the ⁵⁷Fe nucleus and, thus, decreases the isomer shift of **4** relative to that of **1**.

Sandwiches **1** and **4** may be regarded as iron(+III) and iron(+IV) complexes. The isomer shift of **1** may indeed argue for iron(+III). However, with respect to **4** it should be noted that isomer shift values for comparable iron(IV) complexes are unavailable. Mössbauer spectroscopic data for related low-oxidation state complexes are scarce, and a firm correlation between isomer shifts and iron oxidation states is not established for organoiron compounds. Therefore, it remains difficult to assign the oxidation states to iron in **1** and **4** on the basis of the Mössbauer spectroscopic results alone.

Electronic structures of 1–5: To gain insight into the electronic structures of complexes **1–5** we performed a density functional theory (DFT) study. For reasons of computational efficiency, we decided to use truncated models [Fe(η^4 -

P₂C₂Me₂)₂][−] (**1'**), [Co(η^4 -P₂C₂Me₂)₂][−] (**2'**), [Fe(η^4 -P₂C₂Me₂)₂] (**4'**), and [Co(η^4 -P₂C₂Me₂)₂] (**5'**) for which the bulky alkyl substituents in **1–5** were replaced by methyl groups. The model geometries (D_{2d} symmetry), optimized at the OPBE/TZ2P level of theory by using ADF,^[35–37] reproduce the structural features of **1–5** very well. The calculations gave a significant energetic preference for the doublet state of 17-electron complex **1'** over both the quartet ($\Delta E = 30.4$ kcal mol^{−1}) and the sextet ($\Delta E = 64.0$ kcal mol^{−1}). Similar energy differences were found for 16e **4'** for which the triplet ground state is favored over both the open-shell singlet and the quintet by 20.0 and 37.6 kcal mol^{−1}, respectively. Molecular orbital (MO) analysis of **1'** and **5'**, showed dominant metal $d_{x^2-y^2}$ contributions to the singly occupied molecular orbital (SOMO, **1'**: 84% $d_{x^2-y^2}$, **5'**: 55% $d_{x^2-y^2}$). The two singly occupied MOs of **4'** also display the most significant contributions from the iron orbitals (SOMO-1: 65% d_{z^2} , SOMO: 65% $d_{x^2-y^2}$).

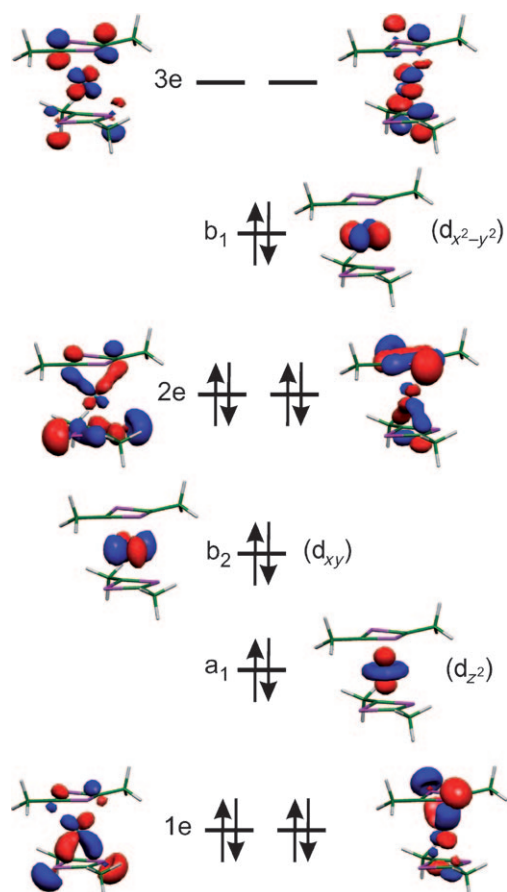
We examined the ground state electronic structures of models **1'**, **2'**, **4'**, and **5'** in greater detail at the spin-unrestricted B3LYP^[38] level of theory. Attempts to find low-energy broken-symmetry states^[39,40] were unsuccessful. All energetically low-lying states feature slightly increased (<9%) expectation values of the \hat{S}^2 operator, pointing to the absence of ligand radicals.^[40] The values and the shape of the atomic spin density distributions are in good agreement with metal-based radicals for **1'**, **4'**, and **5'** (see Figure S5 in the Supporting Information).

Compositions of the quasi-restricted^[41] frontier MOs with substantial metal character are collected in Table 5. For simplicity, we begin our discussion with the diamagnetic 18-electron complex [Co(η^4 -P₂C₂Me₂)₂][−] (**2'**). Three doubly occupied d_{xy} (b_2), d_{z^2} (a_1), and $d_{x^2-y^2}$ (b_1) orbitals can be clearly identified within the frontier orbitals of **2'** (Figure 7). In contrast to ferrocene, the d_{xy} and $d_{x^2-y^2}$ orbitals have different symmetry and are thus not degenerate. The degenerate d_{xz} and d_{yz} orbitals of e symmetry are highly delocalized over several MOs and are discussed below.

To gain insight into the electronic spectrum of **2'** we performed an excited state calculation at the B3LYP-TD-DFT level of theory.^[38,42] The calculated UV/Vis spectrum closely resembles the experimental ones of **2** and **3** (Figure 3 and Figure S6 in the Supporting Information). The calculated states at 20212 and 29466 cm^{−1} mainly arise due to excitations from d_{xy} (b_2), d_{z^2} (a_1) and $d_{x^2-y^2}$ (b_1) type orbitals to the degenerate unoccupied 3e orbital. The latter orbital displays substantial ligand character (Table 5). To a first approximation, these transitions may therefore be regarded as metal-to-ligand charge transfer (MLCT). The state at 31452 cm^{−1} essentially arises from the 1e→3e transition and may be assigned to a delocalized $\pi(\text{ML}) \rightarrow \pi^*(\text{ML})$ transition. The 1e and the 3e orbitals show contributions from both metal and

Table 5. Composition of the frontier quasi-restricted molecular orbitals with significant metal d-character (spin-unrestricted B3LYP-DFT calculations, Löwdin populations).

orbital	[Fe(P ₂ C ₂ Me ₂) ₂] [−] (1')			[Co(P ₂ C ₂ Me ₂) ₂] [−] (2')			[Fe(P ₂ C ₂ Me ₂) ₂] (4')			[Co(P ₂ C ₂ Me ₂) ₂] (5')		
	metal contr. [%]	compos.	occup.	metal contr. [%]	compos.	occup.	metal contr. [%]	compos.	occup.	metal contr. [%]	compos.	occup.
3e (LUMO)	41	d _{xz} +d _{yz}	0	35	d _{xz} +d _{yz}	0	51	d _{xz} +d _{yz}	0	30	d _{xz} +d _{yz}	0
b ₁	96	d _{x²−y²}	1	88	d _{x²−y²}	2	96	d _{x²−y²}	1	96	d _{x²−y²}	1
a ₁	82	d _{z²}	2	78	d _{z²}	2	92	d _{z²}	1	77	d _{z²}	2
2e	17	d _{xz} +d _{yz}	2	12	d _{xz} +d _{yz}	2	18	d _{xz} +d _{yz}	2	9	d _{xz} +d _{yz}	2
b ₂	78	d _{xy}	2	76	d _{xy}	2	81	d _{xy}	2	69	d _{xy}	2
1e	27	d _{xz} +d _{yz}	2	34	d _{xz} +d _{yz}	2	20	d _{xz} +d _{yz}	2	45	d _{xz} +d _{yz}	2

Figure 7. Qualitative MO scheme for **2'**.

ligand orbitals (Figure 7) with 1e being π bonding with respect to the metal-ligand bond and 3e π antibonding. Higher energy states at 35460 and 36419 cm^{-1} are of a complicated origin, with major contributions from the $b_2 \rightarrow a_1$ (MLCT) transition. Finally, the states at 38489 and 37974 cm^{-1} may be assigned to transitions from the occupied 1e and 2e orbitals to unoccupied a_1 and b_2 orbitals, which display ligand π^* character. We conclude that the visible part of the spectrum of **2'** clearly originates from MLCT, whereas intraligand $\pi \rightarrow \pi^*$ transitions play an important role in the UV spectral region.

Upon **2' → 5'** one-electron oxidation, the $d_{x^2-y^2}$ orbital in [Co(η^4 -P₂C₂Me₂)₂] (**5'**) becomes singly occupied (see Figure S7 in the Supporting Information); the composition of

the frontier orbitals does not change. Neutral 17-electron cobalt complex **5'** is isoelectronic with the anionic iron complex [Fe(η^4 -P₂C₂Me₂)₂][−] (**1'**). Both complexes show a very similar composition of the frontier orbitals (Figure S7). One-electron oxidation of **1'** produces 16-electron complex [Fe(η^4 -P₂C₂Me₂)₂] (**4'**), which features singly occupied $d_{x^2-y^2}$ and d_{z^2} orbitals (Figure 8). Population analyses of the individual d orbitals confirm that the *total* d electron density is reduced upon oxidation of **1'** and **2'** (Table 6). However, this depletion of the total d orbital charge amounts to far less than one electron due to charge transfer. As a consequence of π bonding, the occupations of the d_{xz} and d_{yz} orbitals actually *increase* upon oxidation of **1'** and **2'** (Table 6). This

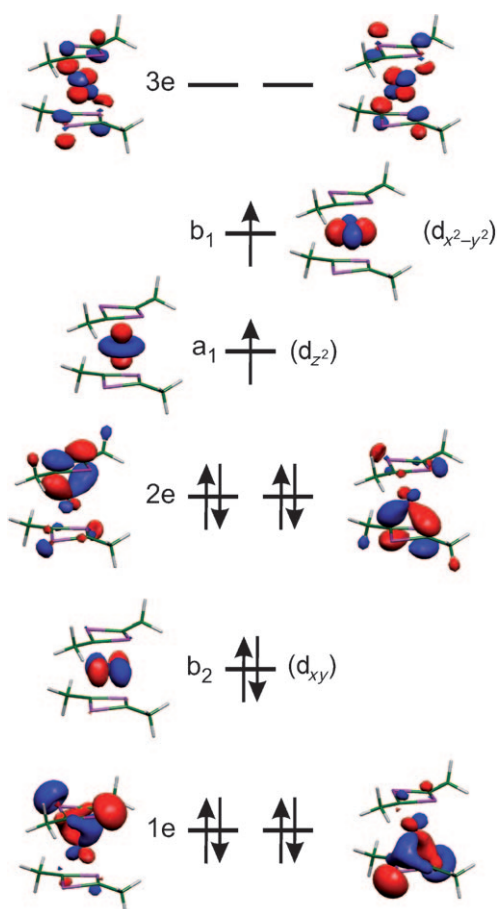
Figure 8. Qualitative MO scheme for **4'**.

Table 6. Reduced orbital charges and orbital spin densities (spin-unrestricted B3LYP-DFT calculations, Löwdin populations).

	[Fe(P ₂ C ₂ Me ₂) ₂] [−] (1')		[Co(P ₂ C ₂ Me ₂) ₂] [−] (2')		[Fe(P ₂ C ₂ Me ₂) ₂] (4')		[Co(P ₂ C ₂ Me ₂) ₂] (5')	
	electron	spin	electron	spin	electron	spin	electron	spin
d _{z²}	1.93	0.02	1.95	0	1.10	0.90	1.97	0.01
d _{xz}	1.21	0.14	1.28	0	1.45	0.20	1.50	0.13
d _{yz}	1.21	0.14	1.28	0	1.45	0.20	1.50	0.13
d _{x²−y²}	1.04	0.96	1.99	0	1.04	0.96	1.05	0.95
d _{xy}	1.71	0.05	1.67	0	1.79	0.07	1.86	0.02
Σd _i	7.11	1.31	8.18	0	6.85	2.32	7.86	1.24
M _{total} ^[a]		1.33		0		2.37		1.26
L _{total} ^[b]		−0.33 ^[c]		0		−0.37 ^[c]		−0.26 ^[c]

[a] The total spin density at metal ion including s and p orbitals. [b] The total spin density at the ligands.

[c] Due to spin polarization.

finding correlates well with the observed trend in the Mössbauer isomer shifts for complexes **1'** and **4'** (vide supra).

Our population analysis, Table 5, shows that b₂ (d_{xy}), a₁ (d_{z²}), and b₁ (d_{x²−y²}) are essentially metal-centered. Intermediate-spin d⁴ (**4'**), low-spin d⁵ (**1'** and **5'**), and low-spin d⁶ (**2'**) configurations should be assigned to the metal if the d_{xz} and d_{yz} orbitals remained unoccupied. Fully occupied d_{xz} and d_{yz} orbitals would result in low-spin d⁸ (**4'**), d⁹ (**1'** and **5'**), and d¹⁰ (**2'**) electronic configurations for the metal ions. However, owing to the mentioned interaction between the d_{xz} and d_{yz} metal orbitals (e symmetry) and ligand π orbitals, it is difficult to determine the exact d occupations of the metal atoms. The occupied 1e orbitals feature a pronounced d_{xz}/d_{yz} character, which is somewhat higher in the cobalt compounds **2'** and **5'** (34 and 45 %, Table 5) as compared to the Fe complexes **1'** and **4'** (27 and 20 %). The unoccupied 3e orbitals also feature substantial metal character (**1'**: 41 %, **4'**: 51 %, **2'**: 35 %, **5'**: 30 %).

Analysis of reduced orbital charges and orbital spin densities yields insight into the electron (charge) and spin populations of each metal d orbital.^[43,44] An electron population of two and a spin population of zero are benchmarks for a fully occupied d orbital. An electron population of one and a spin population of one indicate a singly occupied orbital, whereas the electron and spin populations are both zero for unoccupied orbitals. In our experience, the actual populations can deviate in transition metal complexes from the given ideal values, owing to charge transfer and spin-polarization effects, but the trend is easy to follow.^[43]

For example, the one-electron oxidation **1'**→**4'** is accompanied by a large decrease of the d electron population (1.93→1.10) and a simultaneous increase of the spin population (0.02→0.90) of the d_{z²} orbital (Table 6). It immediately follows that the **1'**→**4'** oxidation therefore corresponds to a metal-based (d_{z²})²→(d_{z²})¹ oxidation. Analogously, the one-electron oxidation **2'**→**5'** is a metal-based (d_{x²−y²})²→(d_{x²−y²})¹ redox event. It is now revealing to analyze the “problematic” d_{xz} and d_{yz} orbitals in **1'**, **2'**, **4'**, and **5'** in the same manner. The spin populations do not exceed 0.20 (Table 6). This is a strong indication that these orbitals should be either fully occupied or unoccupied. However, the electron populations of 1.21–1.50 for d_{xz}/d_{yz} are much lower than the 1.7–2.0 typically found for doubly occupied d orbitals, but

much higher than expected for unoccupied orbitals (eventually 0.0 for a totally ionic system).

Owing to the covalent nature of the metal-ligand bonding a “black or white” picture fails to provide an apt description of the electronic structures of complexes **1–5**. Instead, the electronic situation must be described as intermediate between two extreme cases, that is, [Fe^{−I}(L⁰)₂][−]↔[Fe^{III}(L^{2−})₂][−] for **1**, [Co^{−I}(L⁰)₂][−]↔[Co^{III}(L^{2−})₂][−] for **2**, and **3**, [Fe⁰(L⁰)₂][−]↔[Fe^{IV}(L^{2−})₂][−] for **4**, [Co⁰(L⁰)₂][−]↔[Co^{IV}(L^{2−})₂][−] for **5**, for which L⁰ is the neutral diphosphacyclobutadiene ligand (P₂C₂R₂) and L^{2−} represents the doubly reduced form (P₂C₂R₂)^{2−}. The bonding situation may be understood in terms of a low-valent metal ion that is stabilized by very strong π-acceptor ligands, L⁰, or, alternatively, as a high-valent metal ion that interacts with two very strong π donors, L^{2−}. The two scenarios are essentially equivalent. In both cases, significant electron transfer results in considerable, though incomplete, population of the metal d_{xz}/d_{yz} orbitals as shown by our calculations.

Conclusion

Reactions of phosphalkynes with metalates [M(η⁴-C₁₀H₁₄)₂][−] (M=Fe, Co) yield homoleptic sandwich complexes [M(η⁴-P₂C₂R₂)₂][−], which are formed by means of head-to-tail cyclodimerization of the phosphalkyne at the iron or cobalt center. It should be noted that the related reaction of [Fe(η⁴-C₁₀H₁₄)₂][−] with diphenylacetylene yielded an arene complex through alkyne cyclotrimerization instead.^[45] Complexes [Fe(η⁴-P₂C₂tBu₂)₂][−] (**1**), [Co(η⁴-P₂C₂tBu₂)₂][−] (**2**), and [Co(η⁴-P₂C₂tBu₂)₂][−] (**3**) have been fully characterized spectroscopically. Electrochemical and preparative investigations show that, owing to their electron-rich nature, anions **1** and **2** are readily and reversibly oxidized to neutral sandwiches [M(η⁴-P₂C₂tBu₂)₂] (**4**: M=Fe, **5**: M=Co). Complexes **1–5** feature essentially D_{2d}-symmetric sandwich structures with η⁴-coordinated 1,3-diphosphacyclobutadiene ligands. There is little structural change on oxidation of anions **1** and **2**. Density functional studies show similar molecular orbital compositions for both neutral and monoanionic sandwiches. The highest occupied molecular orbitals display dominant metal character. This observation is nicely corroborated by the EPR spectra of the 17-electron species **1** and **5**, which are consistent with the d_{x²−y²} character of the SOMOs. The isomer shifts of monoanion [Fe(η⁴-P₂C₂tBu₂)₂][−] (**1**) agree well with the shifts of ferrocenium-like iron(III) complexes. However, the DFT calculations clearly show that covalent metal-ligand π bonding is highly significant in these complexes. It is therefore equally appropriate to assign the +III or the −I oxidation state to the

metal centers in anions **1–3**, and oxidation state +IV or 0 to the metal atoms in **4** and **5**. In the former case, electroneutrality^[46] of a high-valent metal ion will be maintained by π donation from the ligand, whereas, in the latter case, excessive charge on a low-valent metal center will be dissipated by metal–ligand π backbonding.

With this work, the properties of a series of homoleptic diphosphacyclobutadiene complexes have been established for the first time. Syntheses, structures, spectroscopic characteristics, and bonding of these complexes are now well-understood. In addition to the homoleptic species described herein, related heteroleptic sandwich anions have very recently become accessible as well.^[47] Future challenges clearly lie in the application of the diphosphacyclobutadiene sandwiches, for example, as building blocks of more elaborate supramolecular structures and multimetallic arrangements. Investigations towards these goals are on-going.

Experimental Section

All experiments were performed under an atmosphere of dry argon, by using standard Schlenk and glovebox techniques. Solvents were purified, dried, and degassed by standard techniques. NMR spectra were recorded (298 K) by using Bruker Advance 250 (³¹P; 85% H₃PO₄) and MSL 400 spectrometers (¹H, ¹³C; SiMe₄), internally referenced to residual solvent resonances. IR spectra were recorded by using a Shimadzu FTIR-84005 spectrophotometer. EI mass spectrometry was performed by using a JEOL JMS SX/SX 102 A four-sector mass spectrometer, coupled to a JEOL MS-MP9021D/UPD system program. Melting points were measured on samples in sealed capillaries and are uncorrected. Compounds *t*Bu–C≡P,^[16] Ad–C≡P,^[17] [K([18]crown-6)(thf)₂][Fe(η^4 -C₁₄H₁₀)₂],^[18] and [K([18]crown-6)(thf)₂][Co(η^4 -C₁₄H₁₀)₂]^[19] were prepared according to literature procedures. [Cp₂Fe]PF₆ and [Cp₂Fe] were purchased from Aldrich and used as received.

EPR spectroscopy: Experimental X-band EPR spectra were recorded by using a Bruker EMX spectrometer equipped with a He temperature control cryostat system (Oxford Instruments). The spectra were simulated by iteration of the anisotropic *g* values, (super)hyperfine coupling constants, and line widths by using the EPR simulation program W95EPR, which is available upon request from Prof. Frank Neese, University of Bonn.

Mössbauer spectroscopy: The Mössbauer spectra of **1** have been measured between 4.2 and 265 K and the spectrum of **4** has been measured at 77 K on constant-acceleration spectrometers, which utilized a rhodium matrix cobalt-57 source and were calibrated at 295 K with α -iron powder. The Mössbauer spectral absorbers were prepared and mounted in the cryostat under an atmosphere of dinitrogen. The relative statistical errors are ± 0.005 mm s^{−1} for the isomer shifts and quadrupole splittings and ± 0.005 (%) (mm s^{−1}) for the total spectral absorption area; double the statistical error associated with the relaxation frequencies are given in Table 3; the absolute errors are approximately twice the statistical errors indicated here.

Cyclic voltammetry and spectroelectrochemistry: Cyclic voltammograms were recorded by using an EG&G PAR model 283 potentiostat operated with the PAR Power CV software. The single-compartment air-tight electrochemical cell contained a 0.42 mm² Pt microdisc working electrode polished between scans with a 0.25 μ m diamond paste (Oberflächentechnologien Ziesmer, Kempen, Germany), a Pt wire auxiliary electrode and an Ag wire pseudoreference electrode (combined with the ferrocene/ferrocenium (Fc/Fc⁺) redox couple used as an internal reference). The saturated calomel electrode (SCE) shows a potential of −0.45 V against Fc/Fc⁺ in dichloromethane.

Thin-layer UV/Vis spectroelectrochemistry was performed by using an optically transparent electrochemical (OTTLE) cell equipped with Pt

minigrid working and auxiliary electrodes, an Ag microwire pseudoreference electrode and CaF₂ windows.^[48] Thin-layer cyclic voltammograms were recorded in the course of each OTTLE experiment for a precise potential control achieved with a PA4 potentiostat (EKOM, Polná, Czech Republic), and for monitoring the progress of the electrolyses by decreasing Faradaic current. The spectroelectrochemical samples were approximately 10^{−3} M in the studied complex and 3 × 10^{−1} M in the supporting electrolyte. UV/Vis spectra of the electrolyzed solutions were obtained by using a HP 8453 A diode array spectrophotometer.

Theoretical calculations: Geometry optimizations of **1'**, **2'**, **4'**, and **5'** were performed in *D*_{2d} symmetry by using ADF2007.01.^[35] The exchange-correlation potential is based on the GGA exchange functional OPTX in combination with the non-empirical PBE (OPBE) and a non-contracted triple-zeta valence-plus-2-polarization STO (TZ2P) basis set was used for all atoms.^{[37],[38]} The inner core electrons of carbon (1s), phosphorus and iron (1s, 2s, 2p) were kept frozen. The truncated X-ray structures of **1**, **2**, **4**, and **5** were used as the starting geometries. All optimized structures were verified as minima by frequency calculations (no imaginary frequencies). For the electronic structures and Mössbauer spectroscopic parameters, single-point calculations were then performed on the optimized geometries using the program package ORCA 2.6 revision 35^[42] and the B3LYP functional.^[38] Tight convergence criteria were used for the SCF procedure (TIGHTSCF). Triple- ζ basis sets with one-set of polarization functions^[49] (TZVP) were used for iron, cobalt, and the phosphorus atoms, and double- ζ basis sets with one-set of polarization functions^[50] (SVP) were used for all other atoms. The resolution of the identity approximation (RIJONX) was employed^[51,52] with matching auxiliary basis sets.^[52] For calculation of Mössbauer spectroscopic parameters, the “core” CP(PPP) basis set for iron^[53] with enhanced integration accuracy on the metal (SPECIALGRIDINTACC 7) was used. All reduced orbital charges and spin densities^[44] were calculated according to Löwdin population analysis.^[54] The reduced orbital population is defined as a population per angular momentum,^[44] meaning the decomposition of the total spin or charge population at the given atom into the population of *s*, *p*, *d*, and *f* orbitals of the atom. Time-dependent DFT (TD-DFT) calculations were performed by using the B3LYP functional and the conductor-like screening model (COSMO) with THF as a solvent.^[55] The first 90 states were calculated, for which the maximum dimension of the expansion space in the Davidson procedure (MAXDIM) was set to 900. Molecular orbitals and spin densities were visualized with the program Molekel.^[56]

[K([18]crown-6)(thf)₂][Fe(η^4 -P₂C₂*t*Bu₂)] (K1): The phosphalkyne *t*Bu–C≡P (5.00 mL, 10.00 mmol, 2 M solution in hexane) was added dropwise to a deep brown solution of [K([18]crown-6)(thf)₂][Fe(η^4 -C₁₄H₁₀)₂] (2.13 g, 2.48 mmol) in THF (\approx 40 mL) at −78 °C and the mixture was allowed to warm to room temperature overnight. The dark orange solution was filtered, concentrated to approximately 10 mL and toluene (\approx 30 mL) was added. **K1** was isolated as a yellow-orange crystalline solid after storage at −20 °C overnight, washed with toluene (3 × 15 mL) and dried in vacuo. Crystals suitable for X-ray crystallography were grown by layering a THF solution of **K1** with *n*-pentane. Yield 1.41 g (75 %); M.p. slow decomposition > 300 °C; ¹H NMR (250.13 MHz, [D₈]THF): δ = −1.9 (very br s; *t*Bu), 1.73 (br s; THF), 3.72 ppm (br s; THF); elemental analysis (%) calcd for C₃₂H₆₀O₆P₄FeK (*M* = 759.66): C 50.59, H 7.96; found: C 49.74, H 7.95; magnetic susceptibility (Evans method, 25 °C, [D₈]THF): μ_{eff} = 1.77 μ_B ; UV/Vis (THF): λ_{max} (ϵ) = 296 (48100), 383 (10000), 699 nm (310 mol^{−1} L cm^{−1}).

[K([18]crown-6)(thf)₂][Co(η^4 -P₂C₂*t*Bu₂)] (K2): Compound **K2** was prepared by an analogous procedure to **K1** by adding *t*Bu–C≡P (1.05 mL, 2.1 mmol, 2 M solution in hexane) to a deep red-brown solution of [K([18]crown-6)(thf)₂][Co(η^4 -C₁₄H₁₀)₂] (0.46 g, 0.53 mmol) in THF (\approx 8 mL). Yield 0.23 g (48 %) of **K2**; m.p.: slow decomposition > 250 °C; ¹H NMR (250.13 MHz, [D₈]THF): δ = 1.04 (br s, 36H; *t*Bu), 1.71 (br s, 8H, THF), \approx 3.5 (very br. s; [18]crown-6), 3.59 ppm (br s, 8H; THF); ¹³C{¹H} NMR (100.62 MHz, [D₈]THF): δ = 34.1 (s; C(CH₃)₃), 36.3 (s; C-(CH₃)₃), 103.1 ppm (t, ¹J(C,P) = 52.3 Hz; C₂P₂*t*Bu₂); the signals for [18]crown-6 and THF were not observed due to overlap with solvent signals. ³¹P{¹H} NMR (101.23 MHz, [D₈]THF): δ = 2.4 ppm; elemental anal-

ysis (%) calcd for $C_{40}H_{76}O_8P_4CoK$ (**K2**–1THF): C 51.79, H 8.21; found: C 51.53, H 8.57; UV/Vis (THF): λ_{max} (ϵ) = 264 (shoulder), 284 (35500), 329 (8900 mol^{−1} L cm^{−1}), 503 nm (shoulder).

[K([18]crown-6)(thf)₂][Co(η^4 -P₂C₂Ad₂)₂] (K3): Compound **K3** was prepared by an analogous procedure to **K1** and **K2** by adding Ad–C≡P (2.1 mL, 1.04 mmol, 0.5 M solution in hexane) to a deep orange-brown solution of [K([18]crown-6)(thf)₂][Co(η^4 -C₁₄H₁₀)₂] (0.46 g, 0.53 mmol) in THF (\approx 8 mL). Yield 0.24 g (76%) of **K3**; m.p.: slow decomposition > 230 °C; ¹H NMR (250.13 MHz, [D₈]THF/C₆D₆ 1:1): δ = 1.46 (br overlapping s, THF), 1.51 (br overlapping s, THF), 1.5–2.0 (overlapping m, 15H; Ad), 3.21 (very br, [18]crown-6), 3.49 (overlapping br s; THF), 3.52 ppm (overlapping br s; THF); ¹³C{¹H} NMR (100.62 MHz, [D₈]THF/C₆D₆ 1:1): δ = 30.3 (s; C-3, C-5, C-7 of Ad), 37.3 (s; C-1 of Ad), 38.0 (s; C-4, C-6, C-10 of Ad), 46.3 (s, C-2, C-8, C-9 of Ad), 103.8 ppm (t, ¹J(C,P) = 51.3 Hz; C₂P₂Ad₂); ³¹P{¹H} NMR (101.23 MHz, [D₈]THF): δ = −2.6 ppm; elemental analysis (%) calcd for C₆₄H₁₀₀O₆P₄CoK (M = 759.66): C 63.04, H 8.26; found: C 62.37, H 8.20; UV/Vis (THF): λ_{max} (ϵ) = 286 (47400), 330 nm (10900 mol^{−1} L cm^{−1}).

[Fe(η^4 -P₂C₂tBu)₂] (4): [Cp₂Fe]PF₆ (0.050 g, 0.15 mmol) was added to a dark-orange solution of **K2** (0.106 g, 0.14 mmol) in THF (6 mL) and the mixture was stirred at room temperature overnight. The solvent was removed completely, the ferrocene byproduct removed by sublimation (10^{−2} Torr, 50 °C), and the dark residue was extracted into *n*-pentane (10 mL). Concentrating the orange-red extract to about 1 mL yielded red crystals of **3** after storage at −20 °C for several days. Yield 0.023 g (36%). M.p. 184–186 °C (dark oil); ¹H NMR (250.13 MHz, C₆D₆): δ = 2.6 (very br. s; tBu); magnetic susceptibility (Evans method, 25 °C, C₆D₆): μ_{eff} = 2.74 μ_B ; UV/Vis (THF): λ_{max} (ϵ) = 275 (65700), 320 (sh), 443 nm (11000 mol^{−1} L cm^{−1}). HRMS (EI): m/z (%): 456.1 (60); calcd for C₂₀H₃₆P₄Fe: 456.1100; found: 456.1117.

[Co(η^4 -P₂C₂tBu)₂] (5): Complex **5** was prepared by an analogous procedure to **4** by oxidation of **K2** (0.221 g, 0.29 mmol) with [Cp₂Fe]PF₆ (0.099 g, 0.30 mmol) in THF. Yield 0.041 g (31%). M.p. 193–194 °C (dark oil); ¹H NMR (200.13 MHz, C₆D₆): δ = −2.6 ppm (very br s; tBu); magnetic susceptibility (Evans method, 25 °C, C₆D₆): μ_{eff} = 1.73 μ_B ; UV/Vis (THF): λ_{max} (ϵ) = 221 (30700), 284 (37000), 313 (43300 mol^{−1} L cm^{−1}), 440 nm (sh); HRMS (EI): m/z (%): 459 (51); calcd for C₂₀H₃₆P₄Co: 459.10995; found: 459.10973.

X-ray crystallography: Reflections were measured by using a Nonius KappaCCD (**K3**) and a Bruker APEXII (**5**, Table 7) diffractometers with rotating anodes and MoK α radiation (λ = 0.71073 Å). Absorption corrections were performed by using SADABS.^[57] The structures were solved by direct methods and refined against F^2 .^[58] The crystal of **K3** (Table 7) contained large voids (1324 Å³ per unit cell) filled with disordered solvent molecules. Their contribution to the structure factors was secured by back-Fourier transformation using the SQUEEZE routine of PLATON,^[49] resulting in 74 electrons per unit cell. Geometry calculations and check for higher symmetry was performed with PLATON.^[59] Details of the structural analyses of **K1**, **K2** and **4** have been reported previously.^[15] CCDC-771227 (**K3**) and CCDC-771228 (**5**) contain the supplementary crystallographic data for this paper. These data can be obtained free of charge from The Cambridge Crystallographic Data Centre via www.ccdc.cam.ac.uk/data_request/cif.

Acknowledgements

We are indebted to Dr. E. Bill (MPI Mülheim/Ruhr) for measuring the solution Mössbauer spectrum of **K1** and valuable discussions. We thank Dr. E.P.A. Couzijn (VU University Amsterdam) for experimental assistance, Prof. Dr. D. Gudat (Universität Stuttgart) for help with microanalysis, and H. Peeters (Universiteit van Amsterdam) for mass spectrometric measurements. Funding from the DFG (IRTG1444 and WO1496/1–1 to 4–1), the Fonds der Chemischen Industrie (Liebig-fellowships to R.W. and M.M.K.) and PhoSciNet is gratefully acknowledged. M.M.K. is grate-

Table 7. Crystal data and structure refinement of **K3** and **5**.

	K3	5
formula	[C ₂₀ H ₄₀ KO ₈] [C ₄₄ H ₆₀ CoP ₄] + disordered solvent	C ₂₀ H ₃₆ P ₄ Co
cryst. size [mm]	0.48 × 0.27 × 0.27	0.11 × 0.05 × 0.02
color	red	orange
formula weight	1219.35 ^[a]	459.30
space group	C2/c	C2/c
<i>a</i> [Å]	14.5182(1)	18.0153(17)
<i>b</i> [Å]	24.7076(2)	8.8666(9)
<i>c</i> [Å]	20.8839(2)	16.783(2)
β [°]	101.6076(5)	117.0460(10)
<i>V</i> [Å ³]	7338.05(10)	2387.6(5)
<i>Z</i>	4	4
<i>T</i> [K]	150(2)	150(2)
ρ_{calcd} [g cm ^{−3}]	1.10 ^[a]	1.28
refl. collected/2 θ_{max} [°]	47294/54.4	11356/54.88
unique reflections	8360	2715
refl. obs. [$I > 2\sigma(I)$]	6889	2328
no. of parameters	354	186
μ [mm ^{−1}]	0.4 ^[a]	1.0
<i>R</i> 1 [$I > 2\sigma(I)$]	0.0419	0.0362
<i>wR</i> 2 (all data)	0.1294	0.1026
GO of F^2	1.08	1.04
residual density [e Å ^{−3}] (min/max)	−0.41/0.70	−0.32/1.15

[a] Derived values do not contain the contribution of the disordered solvent.

ful to the Max Planck Society for a postdoctoral fellowship. R.W. thanks Prof. Dr. W. Uhl for his generous support.

- [1] a) T. J. Kealy, P. L. Pauson, *Nature* **1951**, *168*, 1039; b) G. Wilkinson, M. Rosenblum, M. C. Whiting, R. B. Woodward, *J. Am. Chem. Soc.* **1952**, *74*, 2125; c) E. O. Fischer, W. Pfab, *Z. Naturforsch. B* **1952**, *7*, 377.
- [2] *Metallocenes* (Eds.: A. Togni, R. L. Halterman), Wiley-VCH, Weinheim, **1998**.
- [3] C. Elschenbroich, *Organometallicchemie*, 6th ed., Teubner-Verlag, Wiesbaden, **2008**, pp. 446–449.
- [4] a) A. Efraty, *Chem. Rev.* **1977**, *77*, 691; b) L. Veiros, G. Dazinger, K. Kirchner, M. C. Calhorda, R. Schmid, *Chem. Eur. J.* **2004**, *10*, 5860, and references therein; c) D. Seyferth, *Organometallics* **2003**, *22*, 2; d) U. H. F. Bunz, *Top. Curr. Chem.* **1999**, *201*, 131.
- [5] Rare examples of homoleptic cyclobutadiene nickel complexes: a) H. Hoberg, R. Krause-Göing, R. Mynott, *Angew. Chem.* **1978**, *90*, 138; *Angew. Chem. Int. Ed. Engl.* **1978**, *17*, 123; b) H. Hoberg, C. Froehlich, *J. Organomet. Chem.* **1981**, *213*, C49.
- [6] a) M. Regitz, *Chem. Rev.* **1990**, *90*, 191; b) A. C. Gaumont, J. Denis, *Chem. Rev.* **1994**, *94*, 1413; c) J. F. Nixon, *Coord. Chem. Rev.* **1995**, *145*, 201; d) *Multiple Bonds and Low Coordination in Phosphorus Chemistry* (Eds.: M. Regitz, O. J. Scherer), Thieme, Stuttgart, **1990**; e) K. B. Dillon, F. Mathey, J. F. Nixon, *Phosphorus: The Carbon Copy*, Wiley, Chichester, **1998**; f) F. Mathey, *Angew. Chem.* **2003**, *115*, 1616; *Angew. Chem. Int. Ed.* **2003**, *42*, 1578.
- [7] The catalytic trimerization of phosphalkynes to triphosphabenzene has also been described: F. Tabellion, C. Peter, U. Fischbeck, M. Regitz, F. Preuss, *Chem. Eur. J.* **2000**, *6*, 4558.
- [8] a) P. Binger, B. Biedenbach, R. Schneider, M. Regitz, *Synthesis* **1989**, 960; b) D. Himmel, M. Seitz, M. Scheer, *Z. Anorg. Allg. Chem.* **2004**, *630*, 1220.
- [9] a) P. Binger, R. Milczarek, R. Mynott, M. Regitz, W. Rösch, *Angew. Chem.* **1986**, *98*, 645; *Angew. Chem. Int. Ed. Engl.* **1986**, *25*, 644; b) P. B. Hitchcock, M. J. Maah, J. F. Nixon, *J. Chem. Soc. Chem.*

- Commun.* **1986**, 737; c) P. Binger, R. Milczarek, R. Mynott, C. Krüger, Y.-H. Tsay, E. Raabe, M. Regitz, *Chem. Ber.* **1988**, 121, 637.
- [10] T. Wettling, G. Wolmershäuser, P. Binger, M. Regitz, *J. Chem. Soc. Chem. Commun.* **1990**, 1541.
- [11] a) P. L. Arnold, F. G. N. Cloke, P. B. Hitchcock, J. F. Nixon, *J. Am. Chem. Soc.* **1996**, 118, 7630; b) F. G. N. Cloke, K. R. Flower, P. B. Hitchcock, J. F. Nixon, *J. Chem. Soc. Chem. Commun.* **1994**, 489; c) A. G. Avent, F. G. N. Cloke, K. R. Flower, P. B. Hitchcock, J. F. Nixon, D. M. Vickers, *Angew. Chem.* **1994**, 106, 2406; *Angew. Chem. Int. Ed. Engl.* **1994**, 33, 2330.
- [12] F. G. N. Cloke, P. B. Hitchcock, J. F. Nixon, D. M. Vickers, *J. Organomet. Chem.* **2001**, 635, 212.
- [13] J. E. Ellis, *Inorg. Chem.* **2006**, 45, 3167.
- [14] E. Urnėžius, W. W. Brennessel, C. J. Cramer, J. E. Ellis, P. v. R. Schleyer, *Science* **2002**, 295, 832.
- [15] Preliminary communications: a) R. Wolf, A. W. Ehlers, J. C. Slootweg, M. Lutz, D. Gudat, M. Hunger, A. L. Spek, K. Lammertsma, *Angew. Chem.* **2008**, 120, 4660; *Angew. Chem. Int. Ed.* **2008**, 47, 4584; b) R. Wolf, J. C. Slootweg, A. W. Ehlers, F. Hartl, B. de Bruin, M. Lutz, A. L. Spek, K. Lammertsma, *Angew. Chem.* **2009**, 121, 3150; *Angew. Chem. Int. Ed.* **2009**, 48, 3104.
- [16] a) G. Becker, G. Gresser, W. Uhl, *Z. Naturforsch. B* **1981**, 36, 16; b) W. Rösch, T. Allsach, U. Bergsträßer, M. Regitz in *Synthetic Methods of Organometallic and Inorganic Chemistry*, Vol. 3 (Ed.: W. A. Herrmann), Thieme, Stuttgart, **1996**, p. 11.
- [17] T. Allsach, M. Regitz, G. Becker, W. Becker, *Synthesis* **1986**, 31.
- [18] W. W. Brennessel, R. E. Jilek, J. E. Ellis, *Angew. Chem.* **2007**, 119, 6244; *Angew. Chem. Int. Ed.* **2007**, 46, 6132.
- [19] W. W. Brennessel, V. G. Young, Jr., J. E. Ellis, *Angew. Chem.* **2002**, 114, 1259; *Angew. Chem. Int. Ed.* **2002**, 41, 1211.
- [20] a) D. Böhm, F. Knoch, S. Kummer, U. Schmidt, U. Zenneck, *Angew. Chem.* **1995**, 107, 251; *Angew. Chem. Int. Ed. Engl.* **1995**, 34, 198; b) F. W. Heinemann, S. Kummer, U. Seiss-Brandl, U. Zenneck, *Organometallics* **1999**, 18, 2021.
- [21] M. Driess, D. Hu, H. Pritzkow, H. Schäufele, U. Zenneck, M. Regitz, W. Rösch, *J. Organomet. Chem.* **1987**, 334, C35.
- [22] The reduction of anion **1** to the hypothetical 18e dianion $[\text{Fe}(\eta^4\text{-P}_2\text{C}_2\text{rBu}_2)_2]^{2-}$ was not observed in the experimental potential window. In contrast, the neutral 18-electron complex $[\text{Fe}(\eta^6\text{-C}_7\text{H}_8)(\eta^4\text{-P}_2\text{C}_2\text{rBu}_2)_2]$ can be reduced reversibly at low temperatures to the 19-electron radical anion $[\text{Fe}(\eta^6\text{-C}_7\text{H}_8)(\eta^4\text{-P}_2\text{C}_2\text{rBu}_2)_2]^-$ (−2.50 V vs. SCE in DME at −60 °C) and also oxidized to the corresponding 17-electron radical cation $[\text{Fe}(\eta^6\text{-C}_7\text{H}_8)(\eta^4\text{-P}_2\text{C}_2\text{rBu}_2)_2]^+$ (+0.55 V vs. SCE in CH_2Cl_2).^[21] The different, more negatively shifted redox potentials of **1** compared to the neutral, heteroleptic species $[\text{Fe}(\eta^6\text{-C}_7\text{H}_8)(\eta^4\text{-P}_2\text{C}_2\text{rBu}_2)_2]$ are most likely a consequence of the different charges and formal metal oxidation states of both complexes. The frontier orbitals of $[\text{Fe}(\eta^6\text{-C}_7\text{H}_8)(\eta^4\text{-P}_2\text{C}_2\text{rBu}_2)_2]$ are not known in detail, but it is expected that the reduction is ligand-centered, whereas the oxidation is metal-centered.
- [23] a) D. Hu, H. Schäufele, H. Pritzkow, U. Zenneck, *Angew. Chem.* **1989**, 101, 929; *Angew. Chem. Int. Ed. Engl.* **1989**, 28, 900; b) U. Zenneck, *Angew. Chem.* **1990**, 102, 171; *Angew. Chem. Int. Ed. Engl.* **1990**, 29, 126.
- [24] a) M. Atanasov, C. A. Daul, M.-M. Rohmer, T. Venkatachalam, *Chem. Phys. Lett.* **2006**, 427, 449; b) M. Atanasov, E. J. Baerends, P. Baettig, R. Bruyndonckx, C. Daul, C. Rauzy, M. Zbri, *Chem. Phys. Lett.* **2004**, 399, 433.
- [25] S. Deblon, L. Liesum, J. Harmer, H. Schönberg, A. Schweiger, H. Grützmacher, *Chem. Eur. J.* **2002**, 8, 601, and references therein.
- [26] a) H. van Willigen, W. E. Geiger, M. D. Rausch, *Inorg. Chem.* **1977**, 16, 581; b) L. Vasquez, H. Pritzkow, U. Zenneck, *Angew. Chem.* **1988**, 100, 705; *Angew. Chem. Int. Ed. Engl.* **1988**, 27, 706; c) W. E. Geiger, P. H. Rieger, C. Corbato, J. Edwin, E. Fonseca, G. A. Lane, J. M. Mevs, *J. Am. Chem. Soc.* **1993**, 115, 2314.
- [27] N. G. Connelly, W. E. Geiger, G. A. Lane, S. J. Raven, P. H. Rieger, *J. Am. Chem. Soc.* **1986**, 108, 6219.
- [28] In these fits the isomer shift, δ , the quadrupole splitting, $e^2Qq/2$, and the relaxation rate, δ , have been varied, whereas the line width has been constrained to 0.30 mms^{−1}, the approximate line width observed for the higher velocity line at all temperatures. Further, the effective hyperfine field has been constrained to 11 T, a field that is consistent with the $S = 1/2$ ground state of **1**. The relaxation of the effective hyperfine field cannot be parallel with the principal axis of the electric field gradient at the iron site as this would yield a symmetric spectrum, but must be transverse to this axis. The value of $e^2Qq/2$ may be either positive or negative if the relaxation is normal to this gradient and along the y or x axis, respectively, that is, in the plane containing the singly occupied $d_{x^2-y^2}$ orbital, and the latter case has been chosen to be consistent with the calculated negative quadrupole splitting, see Table 4; the asymmetry parameter, η , has also been constrained to zero in agreement with the structure of **1** and the calculations.
- [29] S. Dattagupta, M. Blume, *Phys. Rev. B* **1974**, 10, 4540.
- [30] G. K. Shenoy, F. E. Wagner, G. M. Kalvius in *Mössbauer Isomer Shifts*, (Eds.: G. K. Shenoy, F. E. Wagner), North-Holland, Amsterdam, **1978**, p. 49.
- [31] It is well known^[30] that the Mössbauer and Debye temperatures, Θ_M and Θ_D , obtained from the two temperature dependencies, are usually different because they depend on $\langle v^2 \rangle$ and $\langle x^2 \rangle$, respectively, for which $\langle v^2 \rangle$ is the root-mean-square vibrational velocity of the ⁵⁷Fe nuclide and $\langle x^2 \rangle$ is the root-mean-square displacement of the ⁵⁷Fe nuclide; unfortunately, there is no model independent relationship^[30] between these mean-square values. However, the values of these temperatures reported^[32] for other iron complexes indicate that Θ_M , which is more sensitive to the high-frequency phonons, is often up to four times larger than Θ_D .
- [32] T. Owen, F. Grandjean, G. J. Long, K. V. Domasevitch, N. Gerasimchuk, *Inorg. Chem.* **2008**, 47, 8704, and the references therein.
- [33] R. V. Parish in *The Organic Chemistry of Iron*, Vol. 1 (Eds.: E. A. K. von Gostorf, F. Grevels, I. Fischler), Academic Press, New York, **1978**, p. 192.
- [34] R. Deschenaux, M. Schweißguth, M. T. Vilches, A. M. Levelut, D. Hautot, G. J. Long, and D. Luneau, *Organometallics* **1999**, 18, 5553.
- [35] ADF2007: E. J. Baerends, J. Autschbach, A. Bérces, F. M. Bickelhaupt, C. Bo, P. M. Boerrigter, L. Cavallo, D. P. Chong, L. Deng, R. M. Dickson, D. E. Ellis, M. van Faassen, L. Fan, T. H. Fischer, C. Fonseca Guerra, S. J. A. van Gisbergen, J. A. Groeneveld, O. V. Gritsenko, M. Grüning, F. E. Harris, P. van den Hoek, C. R. Jacob, H. Jacobsen, L. Jensen, G. van Kessel, F. Kootstra, E. van Lenthe, D. A. McCormack, A. Michalak, J. Neugebauer, V. P. Nicu, V. P. Osinga, S. Patchkovskii, P. H. T. Philipsen, D. Post, C. C. Pye, W. Ravenek, P. Ros, P. R. T. Schipper, G. Schreckenbach, J. G. Snijders, M. Solà, M. Swart, D. Swerhone, G. te Velde, P. Vernooijs, L. Versluis, L. Visscher, O. Visser, F. Wang, T. A. Wesolowski, E. M. van Wezenbeek, G. Wiesenekker, S. K. Wolff, T. K. Woo, A. L. Yakovlev, T. Ziegler, SCM, Theoretical Chemistry, Vrije Universiteit, Amsterdam, The Netherlands, **2007**.
- [36] N. C. Handy, A. J. Cohen, *Mol. Phys.* **2001**, 99, 403.
- [37] J. P. Perdew, K. Burke, M. Ernzerhof, *Phys. Rev. Lett.* **1996**, 77, 3865.
- [38] a) A. D. Becke, *J. Chem. Phys.* **1993**, 98, 5648; b) C. T. Lee, W. T. Yang, R. G. Parr, *Phys. Rev. B* **1988**, 37, 785.
- [39] a) C. Adamo, V. Barone, A. Bencini, F. Totti, I. Ciofini, *Inorg. Chem.* **1999**, 38, 1996; b) A. P. Ginsberg, *J. Am. Chem. Soc.* **1980**, 102, 111; c) L. Noodleman, *J. Chem. Phys.* **1981**, 74, 5737; d) L. Noodleman, J. G. Norman, J. H. Osborne, A. Aizman, D. A. Case, *J. Am. Chem. Soc.* **1985**, 107, 3418; e) L. Noodleman, E. R. Davidson, *Chem. Phys.* **1986**, 109, 131; f) L. Noodleman, D. A. Case, A. Aizman, *J. Am. Chem. Soc.* **1988**, 110, 1001; g) L. Noodleman, C. Y. Peng, D. A. Case, J. M. Mouesca, *Coord. Chem. Rev.* **1995**, 144, 199; h) A. A. Ovchinnikov, J. K. Labanowski, *Phys. Rev. A* **1996**, 53, 3946; i) D. Herebian, K. E. Wieghardt, F. Neese, *J. Am. Chem. Soc.* **2003**, 125, 10997.
- [40] V. Bachler, G. Olbrich, F. Neese, K. Wieghardt, *Inorg. Chem.* **2002**, 41, 4179.
- [41] F. Neese, *J. Am. Chem. Soc.* **2006**, 128, 10213.
- [42] F. Neese, ORCA—an Ab Initio, Density Functional and Semiempirical Program Package, version 2.6, revision 35; Institut für Physikalische Chemie, Universität Bonn, Germany.

- sche und Theoretische Chemie, Universität Bonn, Germany, July 2007.
- [43] a) M. M. Khusniyarov, E. Bill, T. Weyhermüller, E. Bothe, K. Harms, J. Sundermeyer, K. Wieghardt, *Chem. Eur. J.* **2008**, *14*, 7608; b) M. M. Khusniyarov, T. Weyhermüller, E. Bill, K. Wieghardt, *J. Am. Chem. Soc.* **2009**, *131*, 1208.
- [44] ORCA 2.6 manual, February **2007**, p. 296.
- [45] R. Wolf, N. Ghavtadze, K. Weber, E.-M. Schnöckelborg, B. de Bruin, A. W. Ehlers, K. Lammertsma, *Dalton Trans.* **2010**, *39*, 1453.
- [46] L. Pauling, *The Nature of the Chemical Bond*, 3rd ed., Cornell University Press, Ithaca, New York, **1960**, p. 172f.
- [47] R. Wolf, E.-M. Schnöckelborg, *Chem. Commun.* **2010**, *46*, 2832.
- [48] M. Krejčík, M. Daněk, F. Hartl, *J. Electroanal. Chem. Interfacial Electrochem.* **1991**, *317*, 179.
- [49] A. Schäfer, C. Huber, R. Ahlrichs, *J. Chem. Phys.* **1994**, *100*, 5829.
- [50] A. Schäfer, H. Horn, R. Ahlrichs, *J. Chem. Phys.* **1992**, *97*, 2571.
- [51] a) E. J. Baerends, D. E. Ellis, P. Ros, *Chem. Phys.* **1973**, *2*, 41; b) B. I. Dunlap, J. W. D. Connolly, J. R. Sabin, *J. Chem. Phys.* **1979**, *71*, 3396; c) O. Vahtras, J. Almlöf, M. W. Feyereisen, *Chem. Phys. Lett.* **1993**, *213*, 514.
- [52] a) K. Eichkorn, O. Treutler, H. Ohm, M. Haser, R. Ahlrichs, *Chem. Phys. Lett.* **1995**, *242*, 652; b) K. Eichkorn, F. Weigend, O. Treutler, R. Ahlrichs, *Theor. Chem. Acc.* **1997**, *97*, 119.
- [53] a) F. Neese, *Inorg. Chim. Acta* **2002**, *337*, 181; b) S. Sinnecker, L. D. Slep, E. Bill, F. Neese, *Inorg. Chem.* **2005**, *44*, 2245.
- [54] a) P. O. Löwdin, *J. Chem. Phys.* **1950**, *18*, 365; b) P. O. Löwdin, *Adv. Quantum Chem.* **1970**, *5*, 185.
- [55] A. Klamt, G. Schuurmann, *J. Chem. Soc. Perkin Trans. 2* **1993**, 799.
- [56] S. Portmann, Molekel, version 4.3.win32, CSCS/UNI Geneva, Switzerland, November **2002**.
- [57] G. M. Sheldrick, *SADABS/TWINABS: Area-Detector Absorption Correction*, **1999**, Universität Göttingen, Germany.
- [58] G. M. Sheldrick, *Acta Crystallogr. A* **2008**, *64*, 112.
- [59] A. L. Spek, *J. Appl. Crystallogr.* **2003**, *36*, 7.

Received: July 7, 2010
Published online: December 1, 2010